Si chaque expérience ne permet d'examiner qu'une seule raie de diffraction, en revanche les corrections sont réduites au maximum et l'interprétation est ainsi plus directe et plus précise.

Bibliographie

GUINIER, A. (1956*a*). *Théorie et Technique de la Radiocristallographie*, p. 463. Paris: Dunod.

GUINIER, A. (1956*b*). *J. Metals.* p. 673.

LAMBERT, M. (1958). Thèse Université, Paris.

SEBILLEAU, F. & GUINIER, A. (1952). *C. R. Acad. Sci., Paris*, **235**, 888.

SEBILLEAU, F. (1957). *Achromatisme en rayonnement X. — Application à l'étude des raies de diffraction de la solution solide Aluminium–Cuivre à 4% au cours du durcissement structural.* Publication ONERA No. 87, Paris.

STOKES, A. R. (1948). *Proc. Phys. Soc. Lond.* **61**, 382.

Acta Cryst. (1960). **13**, 339

Diffuse Streaks in the Diffraction Pattern of Vanadium Single Crystals

BY E. SÁNDOR AND W. A. WOOSTER

Crystallographic Laboratory, Cavendish Laboratory, Cambridge, England

(*Received* 11 *May* 1959)

Diffuse streaks observed in the diffraction pattern of 99·6% pure vanadium single crystals have been identified as the diffraction pattern of a separate hexagonal phase, which consists of vanadium atoms in hexagonal close packing with nitrogen atoms in octahedral holes. The hexagonal lattice parameters are:

$$a = 2{\cdot}88 \pm 0{\cdot}01,\ c = 4{\cdot}55_5 \pm 0{\cdot}01\ \text{Å},\ c/a = 1{\cdot}58 \pm 0{\cdot}01\ .$$

In most specimens the hexagonal phase has 12 equally probable different orientations relative to the *bcc* vanadium matrix. The lattice relations of the two phases can be described as follows:

$$(00{\cdot}1)_{c.p.h.} \parallel \{110\}_{b.c.c.} \quad \text{and} \quad [100]_{c.p.h.} \parallel [111]_{b.c.c.}$$

i.e. the most densely populated planes of the two phases and one of their most densely populated rows coincide. One particular vanadium single crystal has been found, in which the hexagonal lattice has 24 different orientations. Possible explanations of the observed lattice relations are discussed.

1. Introduction

During the study of the thermal diffuse scattering of vanadium it has been found that well exposed Laue and oscillation photographs taken from certain 99·6% pure vanadium single crystals showed a number of diffuse streaks in addition to the Laue and Bragg spots due to the b.c.c. vanadium lattice (Sándor & Wooster, 1958). Preliminary studies revealed that the streaks were structural in origin and not connected with the thermal diffuse scattering. Annealing the samples for four hours in a vacuum furnace at 800 °C. did not cause any noticeable change in the appearance of the streaks. Powder samples prepared from the same specimens gave a normal b.c.c. diffraction pattern. The lattice parameter deduced from the powder photographs was $a = 3{\cdot}036 \pm 0{\cdot}002$ Å. This value was checked by two single-crystal measurements, namely:

(i) a back-reflection oscillation photograph on which the 400 Bragg-spots due to Cu $K\beta$ were recorded,

(ii) by measuring the separation of the 110 Kossel lines due to the diffraction of the fluorescent V $K\alpha$ radiation in the specimen. Both methods gave $a = 3{\cdot}035 \pm 0{\cdot}002$ Å.

The results of the lattice-parameter measurements agree well with recent measurements on vanadium

Table 1. *Connection between chemical composition and the diffuse pattern*

Sample type	Average chemical composition in wt.% V	O	N	H	C	Fe	Characteristics of the diffuse pattern	Supplier
1	~ 99·6	0·12	0·21	0·12	0·072–0·080	—	Diffuse streaks present	Mackay Chemicals
2	~ 99·7	0·10–0·13	0·02–0·03	0·004–0·006	0·06	0·05	No diffuse streaks	Vanadium Co. of America

samples containing small amounts of oxygen and nitrogen impurities and are significantly greater than recent values obtained for high-purity vanadium (Beatty, 1952; Seybolt & Sumsion, 1953). According to the chemical analysis, there is a marked difference between the nitrogen content of those samples which show the diffuse streaks and of those which do not, as can be seen from Table 1.

2. Experimental details

The investigation of the diffuse streaks was carried out on five cleavage blocks of vanadium single crystals which were electropolished in the later stages of the work. Four specimens had at least one fairly bright (100) cleavage face of area 12–30 mm.^{2} and the fifth specimen was a small, almost regular parallelepiped of the size $1 \times \frac{1}{2} \times \frac{1}{4}$ mm. The specimens were mounted in a Unicam S-25 single crystal goniometer with one tetrad axis parallel to the rotation axis of the goniometer. The Laue and oscillation photographs were taken with Cu $K\alpha$ radiation using (i) a standard quarter-cylinder camera ($r = 114{\cdot}6$ mm.), (ii) a modified version of the half-cylinder camera ($r = 57{\cdot}3$ mm.) capable of covering the angular range $\theta = 0°$–$77°$ along the equator and (iii) a standard small-cylinder camera ($r = 30$ mm.). The collimators were the usual type with circular apertures of diameter $\frac{1}{2}$–$\frac{1}{4}$–$\frac{1}{2}$ mm. and 1–$\frac{1}{2}$–1 mm. respectively. The X-ray tube was run at 30 kV. and 20 mA. and exposure times varied from 2 to 30 hr.

All photographs were taken on Ilford G X-ray film in light-tight cellulose-triacetate envelope (practically grainless). The envelope was covered with a nickel foil about 0·02 mm. thick, which served as a β-filter and also as an absorber of the strong fluorescent radiation generated in the specimen by the incident X-rays.

During the major part of the work one particular single crystal was used, from which Laue-photographs were taken in steps of 1° from $i = 0°$ to $i = 50°$, i being the glancing angle of the incident X-rays on the reflecting (100) face of the specimen. A few Laue-photographs were taken also in the 50°–90° range of angle i and the whole $i = 0°$–$90°$ range was covered with oscillation photographs. Finally the results thus obtained were checked by selected photographs taken from four other specimens. Three of these control specimens provided the same diffuse pattern as the main specimen; the last one, however, gave a diffuse pattern which differed in more than one respect from the rest. In the following 5 sections we deal only with the common diffuse pattern of the four standard specimens. Most of the results derived here apply also to the diffuse pattern of the exceptional fifth specimen. The features peculiar to the fifth specimen will be discussed in the final section.

3. Description of the common diffuse pattern

The diffuse streaks observed on the Laue and oscillation photographs were all similar in shape: they had the appearance of powder lines with very strong preferred orientation and always occurred in pairs symmetrical with respect to the zero layer line (Fig. 1). As the crystal was rotated about the axis of the goniometer, the diffraction angle of the streaks remained constant, their intensity, however, changed continuously. The stronger streaks were observable over a range of about 5°–6°, having maxima of intensity about the centre of the range. The observed diffuse pattern was practically independent of the particular choice of the reflecting (100) face and also of the tetrad axis parallel to the rotation axis of the goniometer. The estimated integrated intensities were

Fig. 1. Four pairs of diffuse streaks on a Laue-photograph taken from a common specimen. The long arcs are vanadium powder lines due to disturbed surface layers. Axis $[001]_{\text{b.c.c.}}$ parallel to the vertical axis of the goniometer. Glancing angle $i_{100} = 30°\ 33'$.

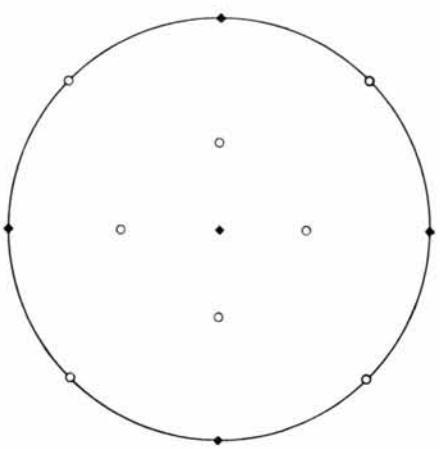

Fig. 2. Stereogram of the $(00{\cdot}2)_{\text{c.p.h.}}$ streak maxima showing the possible orientations of the hexad axes on the upper hemisphere.

the same for all streaks having the same diffraction angle, i.e. lying along the same 'powder line'.

In reciprocal space these streaks are represented by segments of concentric spherical shells around the origin of the reciprocal lattice. To each diffraction angle corresponds a shell of a particular radius. The segments subtend an angle of 5°–6° at the origin of the reciprocal lattice and have maxima of intensity at their centres. Stereograms representing the distribution of the streak maxima on some of these shells can be seen on Figs. 2–5, and Fig. 6 shows the intensity distribution around some of the streak maxima of Fig. 5. The stereograms revealed the following characteristics of the diffuse pattern:

(i) The distribution of the streak maxima in reciprocal space shows cubic symmetry *m3m* relative to the axes of the b.c.c. vanadium lattice.

(ii) Each stereogram can be considered as the superposition of six similar stereograms, each showing hexagonal symmetry around a particular diad axis of the b.c.c. vanadium unit cell. For instance, the streak maxima lying along the dashed circle on Figs. 3–5 show hexagonal symmetry around the $[011]_{b.c.c.}$ diad axis (marked on Figs. 3–5 with the symbol of a hexad axis). This latter observation suggested a hexagonal lattice and in fact all streaks could be indexed on a hexagonal pattern with the unit cell:

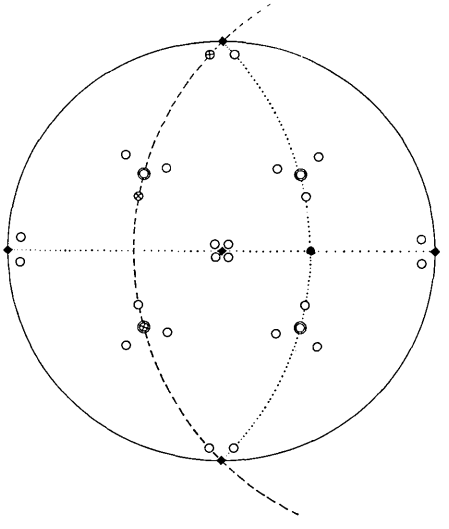

Fig. 3. Stereogram of the $\{11{\cdot}0\}_{c.p.h.}$ streak maxima showing the possible orientations of the $\{100\}_{c.p.h.}$ axes on the upper hemisphere.

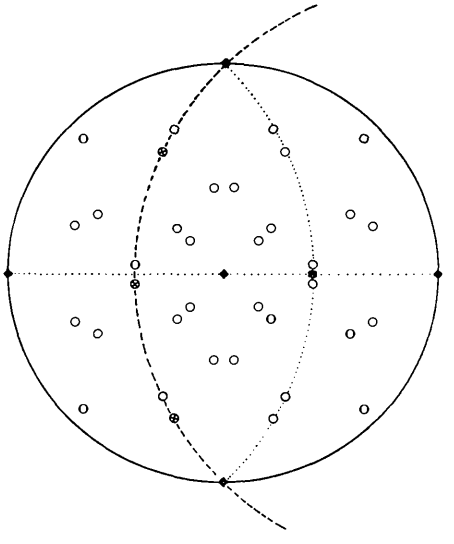

Fig. 4. Stereogram of the $\{10{\cdot}0\}_{c.p.h.}$ streak maxima on the upper hemisphere.

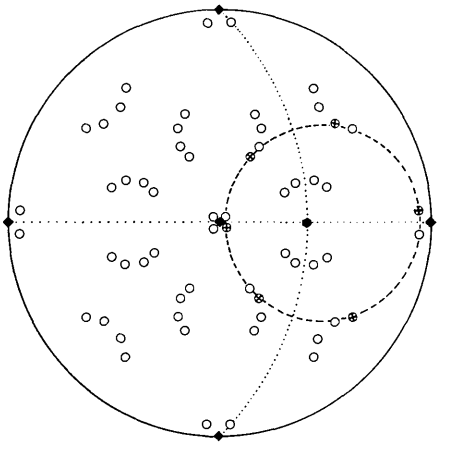

Fig. 5. Stereogram of the $\{10{\cdot}2\}_{c.p.h.}$ streak maxima on the upper hemisphere. The maxima along the dashed circle correspond to those two hexagonal lattices whose common hexad axis is parallel to the [011] face diagonal of the b.c.c. vanadium unit cell.

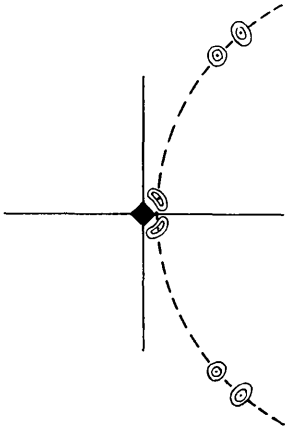

Fig. 6. Intensity distribution of the $\{10{\cdot}2\}_{c.p.h.}$ streaks lying along the dashed circle on Fig. 5. The half-moon-shaped intensity distribution of the two streaks nearest to the centre of the stereogram is due to the fact that the maxima of these streaks are shared by two different lattices and thus the intensity distribution around them is the superposition of two different distributions. The hexad axis of the one lattice is parallel to the $[011]_{b.c.c.}$ direction, the hexad axis of the other parallel to the $[\bar{1}01]_{b.c.c.}$ and the $[10\bar{1}]_{b.c.c.}$ directions respectively.

Table 2. *Diffraction data of the observed diffuse streaks and of* $VO_{0.37}$ *taken from the A.S.T.M. index*

Diffraction data of the hexagonal phase derived from the diffuse streaks					Powder data taken from the ASTM index $VN_{0.37}$		
1	2	3	4	5	6	7	8
hkl	$I_{int.}$	$\theta_{meas.}$	$d_{meas.}$ (Å)	d_c (Å)	$d_{meas.}$ (Å)	I/I_m	I/I_m red.
10·0	*w*	18°	2·495	2·495	2·451	20	25
00·2	*m*	19° 47′	2·28	2·28	2·265	20	75
10·1	*s*	20° 37′	2·19	2·19	2·153	100	62·5
0·2	*ms*	27° 18′	1·68	1·68	1·661	40	25
11·0	*s*	32° 22′	1·44	1·44	1·414	80	100
10·3	*m*	36° 36′	1·29	1·295	1·286	80	50
11·2	*wm*	39° 25′	1·215	1·215	1·198	40	25
20·1	*wm*	39° 55′	1·20	1·20	1·181	20	12·5
00·4	*w*	42°	1·135	1·14	1·132	20	75
20·2	*w*	44° 43′	1·095	1·095	1·077	60	37·5
10·4	*vvw*	48° 5′	1·035	1·035	—	—	—
20·3	*w*	53° 12′	0·963	0·9635	0·951	40	25
21·1	*w*	56° 40′	0·923	0·923	0·906	80	25
11·4	*wm*	59° 40′	0·893	0·893	0·883	80	50
21·2	*vw*	62° 10′	0·872	0·871			
10·5	*w*	64° 22′	0·855	0·8555			
30·0	*wm*	68° 12′	0·830	0·8315			
21·3	*w*	73° 53′	0·803	0·801			

Note.—Column 8 has been derived from column 7 by dividing each figure by the corresponding multiplicity and expressing the result as a percentage of the highest figure. These 'reduced' relative intensities can be compared with the estimated integrated intensities of the diffuse streaks.

$$a=2{\cdot}88\pm0{\cdot}01\ \text{Å},\quad c=4{\cdot}55_5\pm0{\cdot}01\ \text{Å},$$
$$c/a=1{\cdot}58\pm0{\cdot}01,\quad V=32{\cdot}72\pm0{\cdot}24\ \text{Å}^3.$$

The accurate values of the hexagonal lattice parameters were derived from two back reflection photographs taken with the $r=30$ mm. standard Unicam cylinder camera. The photographs contain the three diffuse streaks (10·5), (30·0) and (21·3) having the highest diffraction angles. The hexagonal indices of the observed diffuse streaks, their estimated integrated intensities, the measured diffraction angles, the corresponding lattice spacings and finally the lattice spacings calculated from the cell parameters are listed in the first five columns of Table 2.

4. Interpretation and origin of the diffuse streaks

The indexing of the diffuse streaks revealed two types of systematic absences:

(i) in the $(00{\cdot}l)$ reflections $l=2n$,
(ii) in the $(11{\cdot}l)=(\bar{2}1{\cdot}l)$ reflections $l=2n$.

From the first condition it follows that the hexad axis is a 6_3 screw hexad. As there are no other absences indicating glide planes or other screw axes, the space group must be one of the three following: $P6_3$, $P6_3/m$ or $P6_322$.

The second condition, however, may be identified as the special condition with $l=2n$, if $h-k=3n$, corresponding in all three possible space groups to a twofold special position, in which the atoms form a close-packed-hexagonal arrangement. Owing to the rather high purity of the specimens and the small scattering power of the impurities, we can safely conclude that the c.p.h. framework of the hexagonal phase is formed by vanadium atoms.

Comparing the volume of the b.c.c. unit cell in the parent phase with the volume of the unit cell in the embedded hexagonal phase, we have:

$$V_{c.p.h.}/V_{b.c.c.}=32{\cdot}72/27{\cdot}97=1{\cdot}17\ .$$

As the c.p.h. lattice is a more compact arrangement than the b.c.c., this apparent inversion of the size relations can only mean that the c.p.h. framework of vanadium atoms is expanded by some foreign interstitial atoms.

The chemical analysis of the samples suggests that the most probable interstitial atoms are nitrogen. In the vanadium-nitrogen system there is in fact a hexagonal phase with composition ranging from $VN_{0.37}$ to $VN_{0.43}$ (Hahn, 1949). The lattice parameters, axial ratios and unit-cell volumes corresponding to the two extreme compositions are listed in Table 3. Columns 6–8 of Table 2 give the powder diffraction data of a specimen, whose composition corresponds to $VN_{0.37}$.

Table 3. *Lattice parameters for the two extreme compositions of hexagonal vanadium nitride*

Composition	*a*	*c*	*c/a*	V
$VN_{0.37}$	2·837 Å	4·542 Å	1·602	31·66 Å
$VN_{0.43}$	2·841	4·550	1·602	31·80

Although these lattice parameters are near to our measured values given in the previous section, the deviations are significantly greater than the estimated errors of the respective measurements. One possible explanation for these deviations may be that the oxygen and nitrogen impurities, present probably in

both phases as solid solutions, may increase the lattice parameters of the hexagonal vanadium nitride phase in the same way as they increase the lattice parameters of the b.c.c. vanadium matrix (see Section 1).

The presence of a separate vanadium–nitrogen phase in the specimens would suggest that the solubility of nitrogen in vanadium is less than 0·2 wt.%. This is in agreement with the predictions of Hahn (1949).

The question arises whether the nitrogen atoms associated with the c.p.h. vanadium framework take crystallographically equivalent positions and thus form a regular pattern or are distributed at random in the octahedral holes. As the smallest number of equivalent positions in a c.p.h. unit cell is 2, and the vanadium atoms take a set of such positions, the number of nitrogen atoms in the unit cell must be between $\frac{2}{3}$ and 1, according to the ranges of composition of the hexagonal vanadium nitride (see above). As there are no equivalent positions with such multiplicities in our c.p.h. unit cell, we may conclude that the size of our hexagonal unit cell is inconsistent with an ordered arrangement of the nitrogen atoms.

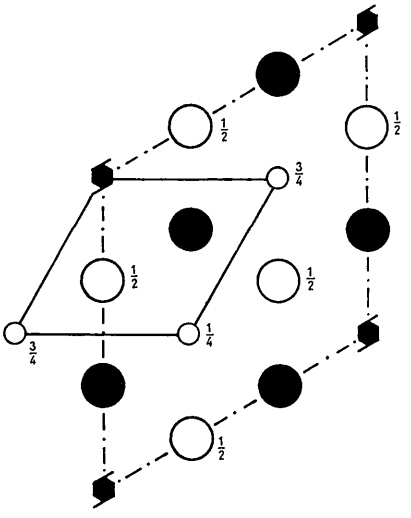

Fig. 7. The (00·1) projection of the hexagonal unit cell derived from the diffuse streaks (full line) and the smallest hexagonal unit cell in the same lattice, which contains two nitrogen atoms in equivalent positions (dash–dot line). The large circles are vanadium atoms, the small circles nitrogen atoms. Full circles indicate atoms in the plane of the projection.

The smallest unit cell in a c.p.h. lattice, which contains two equivalent octahedral holes and in which the ratio of the vanadium atoms to the nitrogen atoms lies within the ranges of composition of the hexagonal vanadium nitride, is three times as great as ours and can be derived from it by rotating the a edge through 30° around the hexad axis and changing its length to $\sqrt{(3)}a$ (see Fig. 7). In the powder pattern of the hexagonal vanadium–nitrogen phase Hahn (1949) in fact observed a very faint 'superstructure line', which could be indexed only by assuming such a larger hexagonal unit cell with six vanadium and two nitrogen atoms. As the contribution of the vanadium atoms to the structure factor of this superstructure line is zero, if the corresponding reflexions were also present in the diffuse pattern, we could conclude that the nitrogen atoms are ordered in the octahedral holes.

Our efforts to find diffuse streaks corresponding to this superstructure line remained inconclusive. On two long-exposure Laue photographs taken in appropriate angular settings it was possible to see two very faint streaks, which could be taken as superstructure reflections, but this identification was hardly convincing. The reason why we could not find enough experimental evidence for the ordering of the nitrogen atoms is fairly obvious. According to the calculations the integrated intensity of the strongest superstructure streak is about one fiftieth of the integrated intensity of the nearest observed diffuse streak. As even this observed diffuse streak is so weak that it can only be seen on long exposure Laue-photographs, there is not much chance that the much weaker superstructure streak would emerge from the continuous background.

5. Lattice relations between the cubic and hexagonal phases

The distribution of the streak maxima on the stereograms of Figs. 3–5 cannot possibly be produced by a single hexagonal lattice of a definite orientation; they must come from a number of identical hexagonal lattices having different orientations relative to the b.c.c. vanadium unit cell. This suggests that the hexagonal vanadium–nitride phase responsible for the diffuse streaks is present in the form of small hexagonal domains of various orientation, scattered all over the b.c.c. vanadium matrix. The orientation of these hexagonal domains can be most conveniently derived from the stereograms of the $(00{\cdot}2)_{\text{c.p.h.}}$ and $(11{\cdot}0)_{\text{c.p.h.}}$ streak maxima. The stereogram of the $(00{\cdot}2)_{\text{c.p.h.}}$ streaks (Fig. 2) is identical with a cubic (110) pole figure. This obviously means that there is a hexad axis parallel to each of the six face diagonals of the b.c.c. unit cell, i.e. that there are six possible orientations for the hexagonal domains. As the integrated intensity of all $(00{\cdot}2)_{\text{c.p.h.}}$ streaks is practically the same, we may conclude that the hexagonal domains are evenly distributed among the six possible orientations.

From the orientation of the hexad axes it follows that for all possible orientations of the hexagonal domains $(00{\cdot}1)_{\text{c.p.h.}} \parallel \{110\}_{\text{b.c.c.}}$, i.e. the most densely populated planes of each hexagonal domain are parallel to one of the most densely populated planes of the b.c.c. vanadium matrix. The atomic arrangement of these two parallel planes can be seen on Fig. 8.

Because of the sixfold symmetry of the hexagonal lattice, we expect to find six evenly distributed $\{11{\cdot}0\}_{\text{c.p.h.}}$ streak maxima along each great circle perpendicular to a possible hexad axis. On Fig. 3,

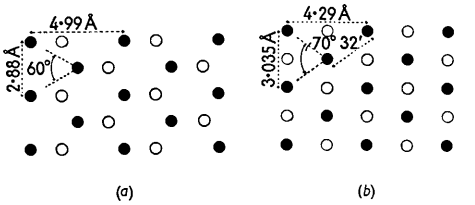

Fig. 8. Arrangement of the vanadium atoms in the most densely populated planes of the embedded hexagonal domains and of the b.c.c. matrix. Full circles indicate atoms in the planes of the paper, open circles atoms above or below the plane of the paper. Characteristic angles of the two arrangements are marked. The distorted hexagonal character of the $\{110\}_{\text{b.c.c.}}$ planes is apparent. (*a*) The (00·1) planes of the hexagonal domains. (*b*) The {110} planes of the b.c.c. vanadium matrix.

however, we find twelve of them, six on the upper hemisphere. (Cf. the six maxima along the dashed great circle). These twelve maxima form two sets of six, i.e. they belong to two different hexagonal lattices which share their hexad axis. (The common hexad axis of the two hexagonal lattices whose $\{11\cdot0\}_{\text{c.p.h.}}$ streak maxima lie along the dashed great circle of Fig. 3, is parallel to the [011] face diagonal of the b.c.c. vanadium unit cell. The maxima corresponding to one of these lattices are marked by a cross. There is one pole in each set which coincides with a particular $[111]_{\text{b.c.c.}}$ pole (see double circles on Fig. 3), which means that each hexagonal lattice domain has a particular $[100]_{\text{c.p.h.}}$ axis parallel to a particular $[111]_{\text{b.c.c.}}$ body diagonal of the vanadium matrix. Thus in each possible orientation of the hexagonal lattice one of its most densely populated rows is parallel to one of the most densely populated rows of the b.c.c. vanadium matrix.

The two hexagonal lattices, having their hexad axis in common, are reflection twins on either of those two mirror planes of the b.c.c. unit cell which pass through the common hexad axis (see dotted lines on Fig. 3). The operation of these mirror planes is equivalent to a 10° (70° 32′ − 60°) rotation around the common hexad axis of the twins.

The lattice relations derived from the stereograms of the $(00\cdot2)_{\text{c.p.h.}}$ and $\{11\cdot0\}_{\text{c.p.h.}}$ streak maxima have been checked by comparing them with the stereograms of the other observed streak maxima. All stereograms gave the same lattice relations within the limits of accuracy. In particular it has been found that:

(i) Stereograms corresponding to higher orders of a particular reflection show the same pattern (e.g. $\{10\cdot0\}_{\text{c.p.h.}}$ and $\{30\cdot0\}_{\text{c.p.h.}}$; $\{10\cdot1\}_{\text{c.p.h.}}$ and $\{20\cdot2\}_{\text{c.p.h.}}$).

(ii) The $\{10\cdot0\}_{\text{c.p.h.}}$ streak maxima lie along the same great circles as the $\{11\cdot0\}_{\text{c.p.h.}}$ streak maxima, in exactly the same sequence, only the two sets of maxima are rotated relative to each other by 30° around the corresponding hexad axis. Hence the different appearance of the two stereograms (Fig. 3 and Fig. 4).

(iii) The $\varphi = \{hk\cdot l\}_{\text{c.p.h.}} \wedge (00\cdot1)_{\text{c.p.h.}}$ angles derived from the stereograms differ by less than 1° from the corresponding calculated values (see Table 4).

The lattice relations discussed above have been derived from the distribution of the streak maxima in reciprocal space; thus they represent only the most probable orientations for the hexagonal lattices. The deviations from them, i.e. the orientations corresponding to the faint outer areas of the diffuse streaks (see Fig. 6), can be attributed to two main factors:

(i) The unit cells near to the boundaries of the hexagonal domains are slightly misoriented and distorted in order to allow a gradual change from the atomic arrangement of one phase to that of the other. This should occur of course on both sides of the phase boundaries. The large size of the vanadium Laue spots together with their faint 'wings', which are also present in the diffraction pattern of the electropolished specimens, seems to support the view that misorientations and distortions are in fact present in the b.c.c. vanadium matrix.

(ii) The hexagonal lattices may contain stacking faults. If the segregation of the hexagonal domains goes according to the mechanism discussed in section 7, the occurrence of such stacking faults is very likely.

6. The relative abundance of the cubic and hexagonal phases

In order to support the chemical evidence and the lattice parameter measurements which indicated that vanadium nitride is responsible for the diffuse streaks, we also investigated whether the intensity of the diffuse streaks is consistent with the abundance of the hexagonal vanadium nitride phase, i.e. with the nitrogen content of the specimens. For this purpose we compared the integrated intensity, $I_{\text{int.}}$, of a $200_{\text{b.c.c.}}$ Bragg reflection with the integrated intensity of that particular $11\cdot0_{\text{c.p.h.}}$ diffuse streak, which is nearest to the chosen $200_{\text{b.c.c.}}$ Bragg reflection. The reasons for the choice of this particular pair are:

(i) Neglecting the scattering of the impurity atoms, which is in any case very small compared with the

Table 4. *Measured and calculated values of the* $\varphi = [hk\cdot l]_{\text{c.p.h.}} \wedge (00.1)_{\text{c.p.h.}}$ *angle for various diffuse streaks*

Miller indices of the streaks		10·0	10·1	10·2	10·3	10·5	20·1	20·3	11·2	21·1
Angle φ	calculated	90°	61° 17′	42° 23′	31° 19′	20° 3′	74° 6′	50° 35′	57° 41′	78° 18′
	derived from the stereogram	90°	60° 45′	41° 45′	31°	20°	73° 30′	50° 30′	57° 30′	78° 15′

scattering of the vanadium atoms, both reflections have the same structure amplitude ($2f_V$).

(ii) The diffraction angles of the two reflections are not very different, (30° 33′ and 32° 22′ respectively); thus all corrections are practically the same for both.

(iii) The $200_{b.c.c.}$ Bragg reflection appears at $i=30°\,33'$ and the $11{\cdot}0_{c.p.h.}$ diffuse streak is observable in the range $i=27°-32°$ with a marked maximum at $i\sim 29{\cdot}5°$. Thus taking a 5° oscillation photograph in the $i=27°-32°$ interval, both reflections can be registered under similar conditions.

From the above discussions it follows that the ratio of the two integrated intensities gives directly the ratio of the number of unit cells for the b.c.c. matrix and for one orientation of the hexagonal lattices. As there are 12 different orientations for the hexagonal lattices and each of them has the same probability, the ratio of the number of unit cells present in the two phases is 12-times less than the measured intensity ratio, i.e.

$$\frac{\text{No of b.c.c. unit cells}}{\text{No of c.p.h. unit cells}}=\frac{1}{12}\frac{I_{\text{int.}}200_{b.c.c.}}{I_{\text{int.}}11{\cdot}0_{c.p.h.}}.$$

Because of the great difference between the integrated intensities, three sets of multiple-film photographs were taken under identical conditions with exposure times in the ratio 1:4:400. By comparing the three sets it could be concluded that the ratio of abundance of the two phases is between 35 and 70, which means that 1·5–3 vanadium atoms out of 100 are associated with the hexagonal phase.

From this observation it follows that if the hexagonal phase is a vanadium–nitrogen phase, the nitrogen content of the specimens should be 0·15–0·35 wt.%, in fair agreement with the chemical analysis.

7. A possible mechanism responsible for the observed lattice relations

Lattice relations, similar to those described in section 5 have been observed by various authors in the martensitic transformation of certain metals and alloys from b.c.c. to c.p.h. structures (Zr: Burgers, 1934; Li: Bowles, 1951; Ti: Newkirk & Geisler, 1953, McHargue, 1953; Cu–Al: Greninger, 1939; Ti–Mn: Liu & Margolin, 1953). Although we have no record of the process of crystallization of our vanadium specimens, the close similarity of the observed lattice relations to the above-mentioned martensitic transformations suggests that a similar mechanism might be operating in both cases. Thus we might assume that when, in the course of crystallization, the hexagonal domains start to segregate from the b.c.c. matrix, this process is governed by rules similar to those which apply to the corresponding martensitic transformation.

The first mechanism for an analogous b.c.c.–c.p.h. martensitic transformation was proposed by Burgers (1934) to explain the transformation of zirconium. Burgers resolved the transformation process into three components:

(i) A homogeneous shear shifting a set of $\{211\}_{b.c.c.}$ planes along their line of intersection with a perpendicular $\{110\}_{b.c.c.}$ plane, i.e. along a $[111]_{b.c.c.}$ body diagonal. This shear leaves unaltered the atomic arrangement in the shifted $\{211\}_{b.c.c.}$ planes. The angle 70° 32′, subtended by the two cubic body diagonals lying in a (110) plane is changed to 60°, which is the characteristic angle in the (00·1) planes of hexagonal lattices.

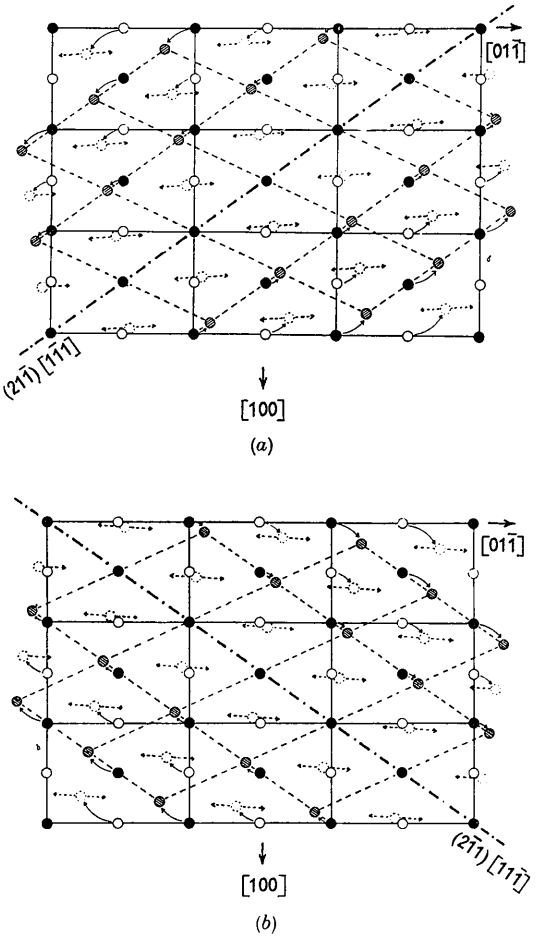

Fig. 9. The movement of atoms in a b.c.c.–c.p.h. martensitic transformation according to Burgers' mechanism.

This shear mechanism is represented in Figs. 9(*a*), (*b*). Both figures show a projection of the b.c.c. structure on the (011) plane. The full circles are atoms in the plane of the paper, the open circles atoms above or below the plane of the paper. The dash-dot lines indicate the directions of those two body diagonals $[1\bar{1}1]_{b.c.c.}$ and $[11\bar{1}]_{b.c.c.}$, in which the two possible invariant planes $(21\bar{1})_{b.c.c.}$ and $(2\bar{1}1)_{b.c.c.}$, both perpendicular to the plane of the paper, intersect the $(011)_{b.c.c.}$ plane. During the shear process the atoms are displaced parallel to $(21\bar{1})_{b.c.c.}$ (Fig. 9(*a*)) and the $(2\bar{1}1)_{b.c.c.}$ planes (Fig. 9(*b*)), these movements are indicated with the full line arrows. The positions of the

atoms after shearing are marked with hatched circles (for the atoms in the plane of the paper) and open dashed circles (for the atoms above or below the plane of the paper). It can be seen that the displacement of any particular atom during the shear process is the bigger, the further away it is from the invariant $\{211\}_{\text{b.c.c.}}$ plane (dash–dot line).

This $\{211\}\langle 111\rangle_{\text{b.c.c.}}$ shear system is the most important component of the whole transformation mechanism and its special choice is based on the following consideration. In order to avoid the accumulation of excessive strain energies, the most likely deformation to occur is that which leaves at least one set of atomic planes in the parent phase undeformed. As the $\{211\}$ planes of the b.c.c. lattice have exactly the same atomic arrangement as the $\{10{\cdot}0\}$ planes of a c.p.h. hexagonal lattice (provided that both lattices are composed of identical spheres, in which case the planes in question consist of rectangles $d \times 1{\cdot}633d$, where d is the diameter of the spheres), a b.c.c.–c.p.h. transformation should leave the $\{211\}_{\text{b.c.c.}}$ planes undeformed.

(ii) The second part of the mechanism is a shift of the atoms above and below the plane of the paper in Fig. 9 to their correct positions in the resulting hexagonal lattice. This can be achieved by two equal but opposite shifts (see the movements of the dashed circles indicated by the dashed arrows on Fig. 9), both producing the same type of c.p.h. lattice. As the two possible shifts are of equal size, it may happen that some of the $\{110\}_{\text{b.c.c.}}$ planes shift the one way, others the opposite way, thus producing stacking faults in the $(00{\cdot}1)$ planes of the hexagonal phase.

(iii) Finally the third component of the transformation is a homogeneous contraction and/or dilatation of the lattice to match the correct lattice parameters of the hexagonal phase.

Burgers' mechanism accounts for all features of the lattice relations observed in our vanadium specimens, including the presence of twins and the 10° difference between their orientations. If the transformation goes according to this mechanism and it is restricted to limited areas of the parent phase, as in the case of our vanadium specimens, in order to minimize the strain energy in the matrix, one would expect that the transformation would produce plate-like hexagonal domains subdivided into thin twin sheets, whose common plane (the habit plane) is parallel to an undistorted $\{211\}_{\text{b.c.c.}}$ plane of the matrix.

In the case of our vanadium specimens there is further support for the view that the segregation of the hexagonal domains goes according to Burgers' mechanism. This is provided by the anomalous diffuse pattern of the fifth specimen, which is discussed in the next paragraph.

8. The anomalous diffuse pattern of the fifth specimen

As already mentioned in section 2, the diffuse pattern of one vanadium cleavage block, a small almost regular parallelepiped, differed in more than one respect from the common diffuse pattern of the other specimens. Some of these differences are shown on the two Laue-photographs of Fig. 10. Fig. 10(*a*) is the common and Fig. 10(*b*) the anomalous diffuse pattern obtained in a $200_{\text{b.c.c.}}$ Bragg-setting. The diffuse streaks on the left-hand side are $\{11{\cdot}0\}_{\text{c.p.h.}}$ streaks, those on the right-hand side $\{10{\cdot}2\}_{\text{c.p.h.}}$ streaks. Similar Laue-photographs have been taken from all six $\{100\}$ faces

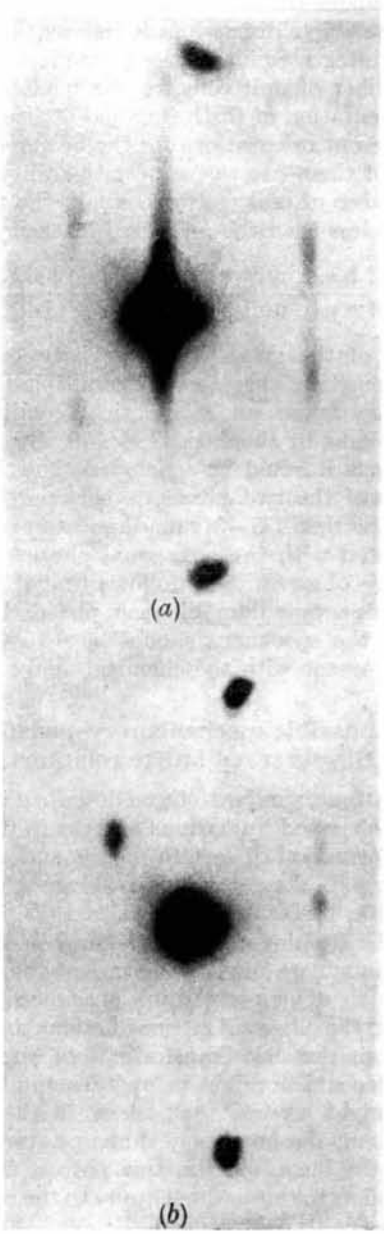

Fig. 10. Corresponding parts of two Laue photographs taken (*a*) from a specimen of the common variety and (*b*) from the fifth specimen, both in a $200_{\text{b.c.c.}}$ Bragg-setting. The diffuse streaks on the left-hand side of both photographs are $\{11{\cdot}0\}_{\text{c.p.h.}}$ streaks, those on the right-hand side $\{10{\cdot}2\}_{\text{c.p.h.}}$ streaks.

of the fifth specimen in two different settings, having first one, then the other tetrad axis lying in the reflecting face coincident with the rotation axis of the goniometer. Although these twelve photographs do not give a comprehensive picture of the anomalous diffuse pattern, they allow us to establish the following special features of this pattern:

(i) Although the arrangement of the diffuse streaks is the same on all 12 Laue photographs, their intensity relations vary with the setting of the crystal. This obviously means that in this particular specimen the various orientations of the hexagonal lattice are not all equally probable. This is well demonstrated on Fig. 10(*b*), where the two $\{11\cdot0\}_{\text{c.p.h.}}$ streaks on the left hand side have very different intensities, the one below the zero layer line being hardly visible at all.

The combined evidence of all twelve Laue photographs suggests that the strong and weak $\{11\cdot0\}_{\text{c.p.h.}}$ streaks are distributed in reciprocal space according to the stereogram in Fig. 11. This stereogram differ from Fig. 3 in that the strong peaks are marked with full circles and the absent or faint streaks with open circles. From Fig. 11 we may conclude that the intensity distribution of the $\{10\cdot2\}_{\text{c.p.h.}}$ diffuse streaks of the fifth specimen has only monoclinic symmetry. The only mirror plane of the intensity distribution is marked on Fig. 11 with a dash–dot line.

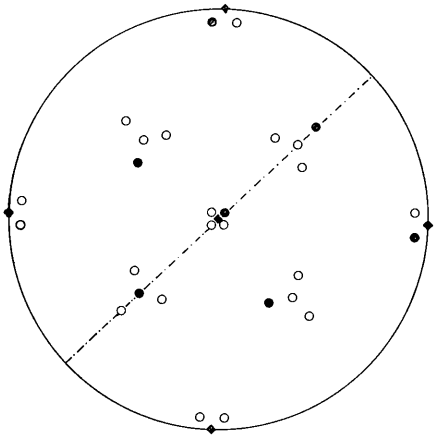

Fig. 11. Stereogram representing the distribution of the strong and weak $\{11\cdot0\}_{\text{c.p.h.}}$ streak maxima of the fifth specimen in reciprocal space.

(ii) There are twice as many $\{10\cdot2\}_{\text{c.p.h.}}$ streaks on Fig. 10(*b*) as there are on Fig. 10(*a*). As this doubling is present on all 12 Laue photographs, we may conclude that in this particular specimen there are twice as many possible orientations for the hexagonal lattice, as in the common specimens, i.e. 24, instead of 12. The central part of the stereogram representing the distribution of the $\{10\cdot2\}_{\text{c.p.h.}}$ peaks of the fifth specimen in reciprocal space can be seen in Fig. 12. The full circles are the common peaks (they correspond on an enlarged scale to the four circles around the centre of Fig. 5) and the dotted circles the additional peaks, present only in the diffuse pattern of the fifth specimen. Fig. 12 shows that the additional

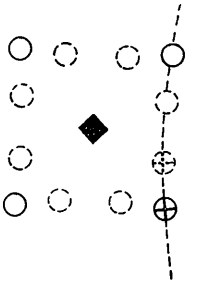

Fig. 12. The central part of the stereogram representing the distribution of the $\{10\cdot2\}_{\text{c.p.h.}}$ streak maxima of the fifth specimen in reciprocal space. The scale of this figure is about ten times as big as that of Fig. 5.

$\{10\cdot2\}_{\text{c.p.h.}}$ peaks of the fifth specimen lie on the same small circles around the hexad axes, as the common $\{10\cdot2\}_{\text{c.p.h.}}$ peaks. (The dashed arc on Fig. 12 corresponds to the dashed small circle on Fig. 5). The angular distance between two consecutive additional $\{10\cdot2\}_{\text{c.p.h.}}$ peaks along the dashed small circle is $\sim 5°$ and both are $\sim 2\cdot5°$ apart from the nearest common peaks. All this suggests that the 24 hexagonal lattices of the fifth specimen have the same six hexad axes

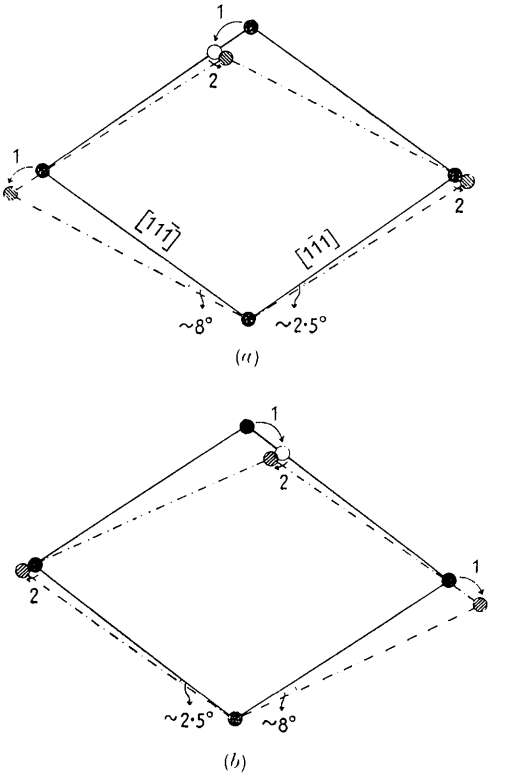

Fig. 13. The operation of the two double shear systems, responsible for the additional $\{10\cdot2\}_{\text{c.p.h.}}$ streaks in the diffraction pattern of the fifth specimen.

as the 12 hexagonal lattices of the common specimens, only in this particular specimen each hexagonal axis is shared by four lattices forming two pairs of reflection twins on the same two mirror planes of the b.c.c. unit cell, as in the case of the common specimens.

For the anomalous diffuse pattern of the fifth specimen we propose the following tentative explanation. In the fifth specimen the shear movement along certain $\{211\}_{\text{b.c.c.}}$ planes meets such a great obstruction that, so far as stored energy is concerned, it is more favourable to stop the shear movement along these planes at a certain point and complete the transformation by a small shear of opposite sense, i.e. by a shear along the other $\{211\}\langle 111\rangle_{\text{b.c.c.}}$ shear system operating in the same $\{110\}_{\text{b.c.c.}}$ plane. By interchanging the sequence and size of the two shifts corresponding to the two components of the double shear system, we get two possible double shear systems, the lattices resulting from them being reflection twins.

The atomic displacements produced by these two possible double shear systems are represented in Figs. 13(*a*), (*b*). The plane of both figures is a (011) plane of the b.c.c. vanadium matrix, the same as in Fig. 9. In order to simplify the representation, both figures show the displacements of only four atoms lying in the $(011)_{\text{b.c.c.}}$ plane (full circles). These four atoms form a parallelogram, whose two sides correspond to the two shear directions $[1\bar{1}1]_{\text{b.c.c.}}$ and $[\bar{1}11]_{\text{b.c.c.}}$ included in the double shear system $(21\bar{1})\ [1\bar{1}1]_{\text{b.c.c.}} + (2\bar{1}1)\ [11\bar{1}]_{\text{b.c.c.}}$. The first displacement of the atoms is indicated by the arrows (1), the second displacement by the arrows (2). In their final positions (hatched circles) these four atoms form a basal rhomb of the product hexagonal lattice, whose sides subtend with the cubic body diagonals $[11\bar{1}]$ and $[1\bar{1}1]$ the angles indicated on the figures.

From the evidence of the diffraction pattern alone we cannot decide what kind of obstruction is responsible for the blocking of the normal shear process. But as the atoms far from the invariant $\{211\}_{\text{b.c.c.}}$ plane (indicated with dash–dot line on Fig. 9) have to move a considerable distance during the shear process, it is not unreasonable to expect that spatial limitations in certain areas of the crystallizing substance might in fact provide such obstruction. Apart from this, the mechanism proposed above accounts for all features of the anomalous diffuse pattern of the fifth specimen and it also provides support for the view that the principal factor in the segregation of the hexagonal phase in the b.c.c. vanadium matrix is a $\{211\}\langle 111\rangle_{\text{b.c.c.}}$ shear system.

We gratefully acknowledge the receipt of a grant from the Department of Scientific and Industrial Research in support of this work. We also wish to acknowledge the help afforded by the Vanadium Corporation of America in supplying vanadium single crystals, by the United Kingdom Atomic Energy Authority, Harwell, and by Mr W. T. Elwell, I. C. I. Metals Division in carrying out the chemical analysis of the samples.

References

Beatty, S. (1952). *J. Metals*, **4**, 987.
Bowles, J. S. (1951). *Trans. Amer. Inst. Min. (Metall.) Engrs.* **191**, 44.
Burgers, W. G. (1934). *Physica*, **1**, 561.
Greninger, A. B. (1939). *Trans. Amer. Inst. Min. (Metall.) Engrs.* **133**, 204.
Hahn, H. (1949). *Z. anorg. Chem.* **258**, 58.
Liu, Y. C. & Margolin, H. (1953). *J. Metals*, **5**, 667.
McHargue, C. J. (1953). *Acta Cryst.* **6**, 529.
Newkirk, J. B. & Geisler, A. H. (1953). *Acta Met.* **1**, 370.
Sándor, E. & Wooster, W. A. (1958). *Nature, Lond.* **182**, 1435.
Seybolt, A. U. & Sumsion, H. T. (1953). *J. Metals*, **5**, 292.